Applied Catalysis B: Environmental 98 (2010) 49–56

Contents lists available at ScienceDirect

Applied Catalysis B: Environmental

journal homepage: www.elsevier.com/locate/apcatb

Palladium–vanadium alloy electrocatalysts for oxygen reduction: Effect of heat treatment on electrocatalytic activity and stability

Shee-Yen Ang, Darren A. Walsh*

School of Chemistry and Faculty of Engineering, The University of Nottingham, Nottingham NG7 2RD, UK

ARTICLE INFO

Article history:
Received 22 January 2010
Received in revised form 22 April 2010
Accepted 26 April 2010
Available online 25 May 2010

Keywords:
Oxygen reduction
Fuel cell
Palladium alloy
Rotating disk electrode

ABSTRACT

Carbon black (Vulcan XC72R)-supported palladium–vanadium electrocatalysts for the oxygen reduction reaction (ORR) were synthesized by wet chemical reduction of metal chloride salts. The nominal compositions of the electrocatalysts were 60:40, 70:30 and 80:20 (Pd/V atomic ratio). The electrocatalysts were treated at a range of temperatures in 10% H_2 in Ar and the effect of heat treatment on particle morphology was characterised using powder X-ray diffraction and transmission electron microscopy. These analyses showed that high temperatures caused an increase in the average particle size. The electrocatalytic activities of the electrocatalysts for the ORR were determined using rotating disk electrode voltammetry, which revealed a marked enhancement in the electrocatalytic activity of the $Pd_{70}V_{30}$ electrocatalyst after heat treatment. The electrochemical stability of the electrocatalysts was examined using an accelerated stability test, which showed a loss of electrochemical surface area upon electrochemical cycling, the extent of which depended on the nominal composition of the electrocatalysts. Electrocatalyst testing after the stability test showed a loss of electrocatalytic performance and microscopic analysis revealed significant morphological changes in the electrocatalyst particle dimensions and dispersion on the carbon support after the stability test.

1. Introduction

The search for novel, inexpensive ORR electrocatalysts for fuel cell cathodes has been an intensely active area of research for a number of years. The ORR occurs slowly at most catalyst surfaces and platinum remains the catalyst of choice within fuel cell cathodes. In recent years, a number of platinum alloys have been developed that offer enhancements in electrocatalytic efficiency and which can reduce costs by lowering the amount of platinum required to drive the ORR [1–3]. Several groups are also developing non-platinum alternatives for ORR electrocatalysis, which include transition metal macrocycles [4] and metal carbides [5]. A number of non-platinum metal alloys have also been studied, the most promising of which are palladium alloys such as PdMo [6], PdCo [7] and PdTi [8] and some of these materials compete with platinum in terms of electrocatalytic activity.

An extremely important consideration in the development of fuel cells is the electrochemical stability of the electrocatalyst, which can drastically affect the fuel cell lifetime. The US Department of Energy has listed several lifetime targets that must be reached before widespread fuel cell commercialization can be realized and these include a 2010/2015 target of 5000 h for PEMFCs in transportation applications and a 2011 target of 40,000 h for integrated stationary PEMFCs [9]. In operational fuel cells, platinum electrocatalyst particles can dissolve and the soluble platinum species can redeposit on adjacent particles leading to particle growth [10]. Migration and coalescence of particles can also occur [11] and these effects can lead to loss of electrochemical surface area and a drop in power output. Recent work has also shown that loss of electrochemical surface area is more significant when the cell potential varies continuously, such as in the stop–start operation of automobiles, than if the cell operates at constant potential [12]. While the majority of investigations into the stability of fuel cell electrocatalysts has involved platinum electrocatalysts, some studies have also shown that palladium-based electrocatalysts may be unstable in acidic media at high potentials [7,13,14]. Therefore, before Pd alloys can become a realistic replacement for platinum in fuel cells, the long-term stability of these catalysts must be evaluated and strategies for enhancing the electrochemical stability must be developed.

A number of publications have appeared describing the activity of platinum–vanadium alloys for the ORR [15,16]. However, to the best of our knowledge, only a single paper has appeared describing the promising activity of palladium–vanadium alloys for ORR electrocatalysis [17]. The effect of heat treatment on the electrochemical performance and durability of these electrocatalysts has not been explored to date and it is important to investigate these effects as heat treatment can alter the elec-

* Corresponding author. Tel.: +44 115 951 3437; fax: +44 115 951 3562.
E-mail address: darren.walsh@nottingham.ac.uk (D.A. Walsh).

0926-3373/$ – see front matter © 2010 Elsevier B.V. All rights reserved.
doi:10.1016/j.apcatb.2010.04.025

trocatalytic performance of fuel cell electrocatalysts dramatically [18].

In this contribution, we describe the synthesis of carbon black (Vulcan XC72R) supported palladium–vanadium alloys with nominal vanadium contents ranging from 20% to 40% and demonstrate that heat treatment has a significant effect on the electrocatalytic performance and durability of these materials during ORR electrocatalysis. Transmission electron microscopy (TEM) and X-ray diffraction (XRD) were used to characterize the morphology of the as-prepared electrocatalyst, which was compared with that of samples of each electrocatalyst subjected to thermal treatment at 300 °C and 500 °C in a reducing atmosphere. The electrocatalytic activity of each electrocatalyst for the oxygen reduction reaction (ORR) in acidic medium was studied using rotating disk electrode (RDE) voltammetry and the effect of heat treatment on the electrocatalytic performance evaluated. The electrochemical stability of the electrocatalysts was also examined using an accelerated stability test in which the potential of the electrocatalysts was cycled repeatedly. This test showed significant differences in the electrochemical stability of the electrocatalysts depending on the nominal composition. Finally, RDE voltammetry and TEM analysis were used to study the effect of potential cycling on the electrocatalyst performance and morphology.

2. Experimental

2.1. Materials and apparatus

All reagents were purchased from Sigma Aldrich and were used as received. Carbon black (Vulcan XC72R) was obtained from Cabot Co. (Boston, Massachusetts). Electrochemical measurements were performed using a Model CHI760C bipotentiostat from CH Instruments (Austin, TX), a 5 mm diameter glassy carbon (GC)–Pt ring rotating ring–disk electrode (RRDE) assembly and Model MSR Modulated Speed Rotator from Pine Instruments (Raleigh, NC).

2.2. Preparation of PdV/C electrocatalysts

The targeted metal loading in each electrocatalyst was 20 wt.%. To prepare each electrocatalyst, the appropriate amounts of palladium(II) chloride and vanadium(II) chloride were dissolved in 100 mL of deionised water in the presence of 120 mg of Vulcan XC72 to obtain nominal PdV compositions of 60:40, 70:30 and 80:20 (atomic ratios). The suspensions were then sonicated for 10 min to achieve uniform dispersions. 0.5 M NaOH was then added drop wise to the suspensions to raise the pH of each to approximately 10. The metal salts were reduced by adding a 10× molar excess of aqueous $NaBH_4$ solution to the suspensions while sonicating. The reactions were left overnight to ensure complete reduction. The solid products were recovered by filtration, washed with deionised water and oven dried at 70 °C.

2.3. Electrocatalyst heat treatment

Each electrocatalyst was heat treated at 300 °C and 500 °C in a tube furnace under flowing 10% H_2 in Ar. The furnace temperature was ramped from room temperature to the appropriate temperature at 10 °C min^{-1} and was then kept constant for 2 h. The samples were then allowed to cool to room temperature under flowing H_2/Ar in the tube furnace.

2.4. Morphological charaterisation of PdV/C electrocatalysts

The electrocatalysts were characterised using TEM and XRD. For TEM analysis, dilute suspensions of each PdV/C electrocatalyst were prepared in acetone. Carbon TEM grids were coated with the suspension and allowed to dry in air before imaging using a FEI Tecnai 12 Biotwin TEM, operated at 120 kV. XRD was performed by bombarding each sample with an X-ray beam from a copper K_α source (λ = 0.154 nm) and recording reflections from 20° to 80° at 0.1° increments.

2.5. Electrochemical charaterisation of PdV/C electrocatalysts

Prior to use, the RDE surface was polished using aqueous suspensions of alumina with successively smaller particle sizes from 1 μm to 0.05 μm, rinsed with deionized water and then sonicated in a small amount of deionized water to remove residual polishing material. During electrochemical experiments, an Ag|AgCl reference electrode and a platinum wire counter electrode were used. However, all potentials in the text are reported vs the standard hydrogen electrode (SHE). Cyclic voltammetry was performed at the same electrode in deoxygenated 0.5 M H_2SO_4 while RDE experiments were performed in O_2-saturated 0.5 M H_2SO_4 at 25 °C.

Catalyst inks were prepared by dispersing the PdV/C electrocatalysts in 80:20 water/ethanol to a concentration of 2 mg mL^{-1}. Nafion (5 wt.% in ethanol) was diluted 1:80 with water and the resulting solution was mixed with an equal volume of the catalyst suspension, giving a PdV/C concentration of 1 mg mL^{-1}. 20 μL of the suspension was drop cast onto the GC surface and the assembly was dried for 20 min at 40 °C. Prior to use, the electrocatalyts were electrochemically cycled in 0.5 M H_2SO_4 between 0.4 V and 0.9 V until a stable cyclic voltammogram (CV) was obtained (approximately 50 cycles). RDE experiments were performed by rotating the electrode (rotation rates are described in the text) and sweeping the potential of the GC disk in a negative potential direction from 0.9 V to 0.0 V at 5 mV s^{-1} and recording the current for oxygen reduction. All RDE measurements were repeated at least twice and the polarisation curves shown in the manuscript are representative of that observed for each electrocatalyst. In RRDE voltammetry experiments, the ring was held at 1.2 V to detect H_2O_2.

3. Results and discussion

3.1. Physical characterization of PdV/C electrocatalysts

Fig. 1 shows representative TEM images of the as-prepared (AP) electrocatalysts, as well as images of the samples subjected to heat treatment. In each case, the metal particles were well dispersed on the carbon support and showed a distribution of particle sizes between 2.0 nm and 13.0 nm. The average particle sizes (based on measuring 50 particles) are shown in Table 1 and Fig. 2 shows particle size distributions for each sample determined from the TEM images. At each composition, heat treatment caused an increase in the average particle size and there was a clear broadening of the particle size distribution. Fig. 3 shows the XRD patterns obtained for the as–prepared electrocatalysts and those treated at each temperature. The pattern obtained for pure Pd is also shown for comparison. Each electrocatalyst yielded a pattern typical of that expected for a face centred cubic (fcc) structure and there was no evidence of any peaks corresponding to V or VO_x, either due to the low concentration of such species or poor crystallinity. In each sample, the reflections were shifted to higher angles compared to pure Pd, indicating a lattice contraction as the smaller V atoms were incorporated into the Pd lattice. The lattice parameter, *a*, was calculated from the XRD data for each electrocatalyst and this data is shown in Table 1. As the treatment temperature was increased to 300 °C and 500 °C, the peaks shifted to higher angles indicating an increase in the degree of alloying at higher temperatures. The crystallite size in each of the samples was estimated using the Scherrer formula and the values are shown in Table 1. The estimated crystallites sizes determined using the Scherrer formula were slightly

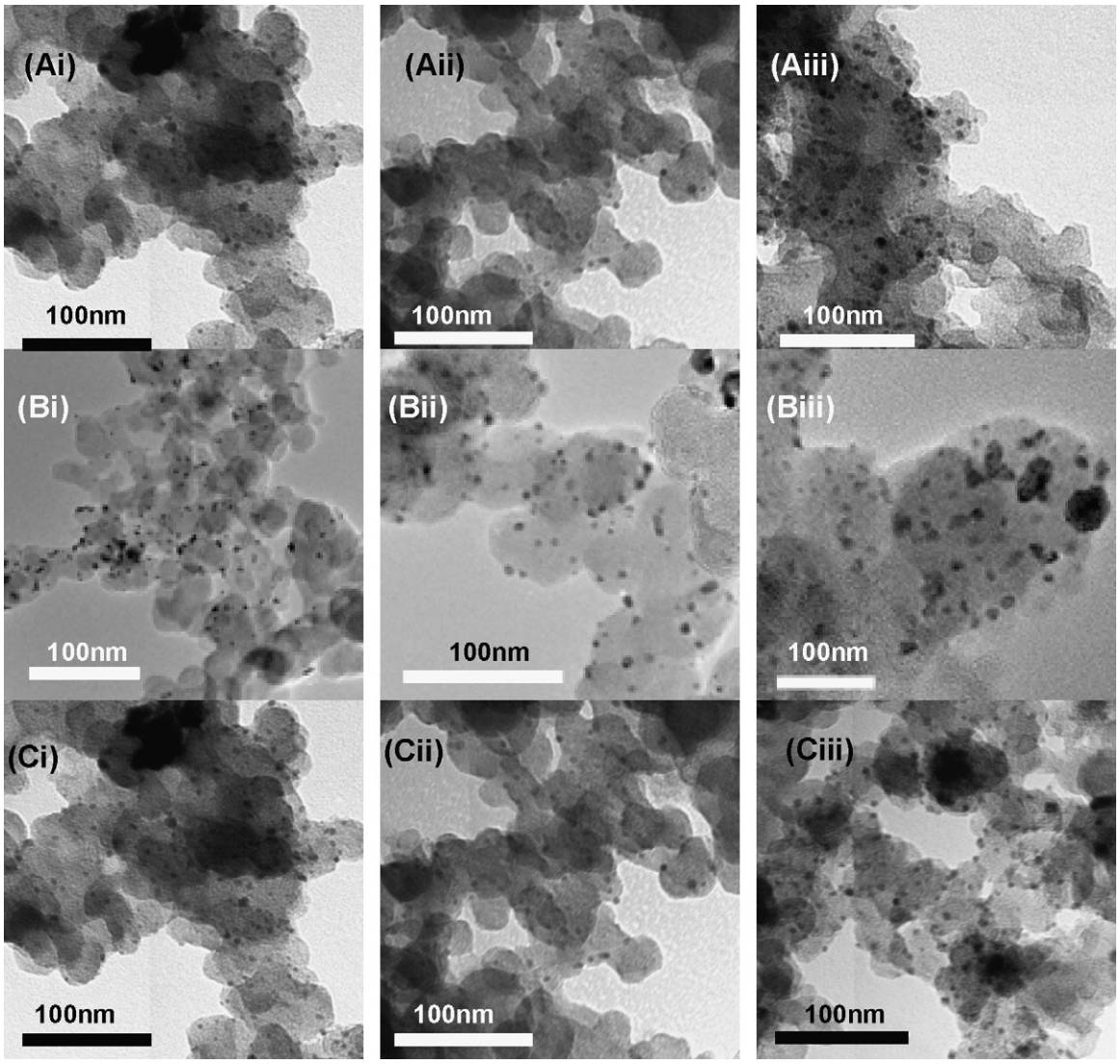

Fig. 1. TEM images of as-prepared (AP) PdV/C electrocatalysts and those heat treated at 300 °C and 500 °C. (Ai) $Pd_{60}V_{40}$(AP), (Aii) $Pd_{60}V_{40}$(300), (Aiii) $Pd_{60}V_{40}$(500), (Bi) $Pd_{70}V_{30}$(AP), (Bii) $Pd_{70}V_{30}$(300), (Biii) $Pd_{70}V_{30}$(500), (Ci) $Pd_{80}V_{20}$(AP), (Cii) $Pd_{80}V_{20}$(300) and (Ciii) $Pd_{80}V_{20}$(500).

larger than the average particle sizes obtained using TEM analysis. However, in general, the same trend was observed as the treatment temperature increased, i.e. the average crystallite size increased with increasing temperature. The only exception was that the average crystallite size of the $Pd_{70}V_{30}$ (500) was slightly lower than that of the $Pd_{70}V_{30}$(300). Given that estimation of the crystallite size from XRD data is subject to error from instrumental line broadening and crystal strain effects [19], this slight difference may be due to error in estimating the average crystal size. Nonetheless, as the XRD-determined average is based on the measurement of millions of particles while the TEM-determined average is based on measuring a relatively small number of particles (50), in the following section we use the XRD-determined average crystallite dimensions in calculating the catalyst surface area.

3.2. ORR electrocatalysis at PdV/C electrocatalysts

Rotating disk electrode (RDE) voltammetry was used to study electrocatalysis of the ORR at each electrocatalyst and Fig. 4 shows typical RDE polarisation curves obtained at 1600 rpm in

Table 1
Characterisation data of the PdV electrocatalysts from TEM and XRD. The first Bragg angle was measured at the (1 1 1) plane at each sample.

Sample	Bragg angle (°)	*d*-spacing (Å)	Lattice parameter *a* (Å)	Particle size (TEM) (nm)	Crystallite size (XRD) (nm)
Pd/C	39.80	2.2619	3.9177		5.3
$Pd_{60}V_{40}$(AP)	40.33	2.2334	3.8683	4.1	5.8
$Pd_{60}V_{40}$(300)	40.38	2.2307	3.8638	4.3	6.4
$Pd_{60}V_{40}$(500)	40.55	2.2218	3.8482	4.5	9.4
$Pd_{70}V_{30}$(AP)	40.11	2.2451	3.8887	3.5	6.1
$Pd_{70}V_{30}$(300)	40.43	2.2281	3.8592	4.0	7.2
$Pd_{70}V_{30}$(500)	40.55	2.2218	3.8482	4.5	6.6
$Pd_{80}V_{20}$(AP)	39.83	2.2603	3.9149	3.7	5.4
$Pd_{80}V_{20}$(300)	39.93	2.2548	3.9055	3.9	7.0
$Pd_{80}V_{20}$(500)	40.13	2.2441	3.8868	4.9	9.0

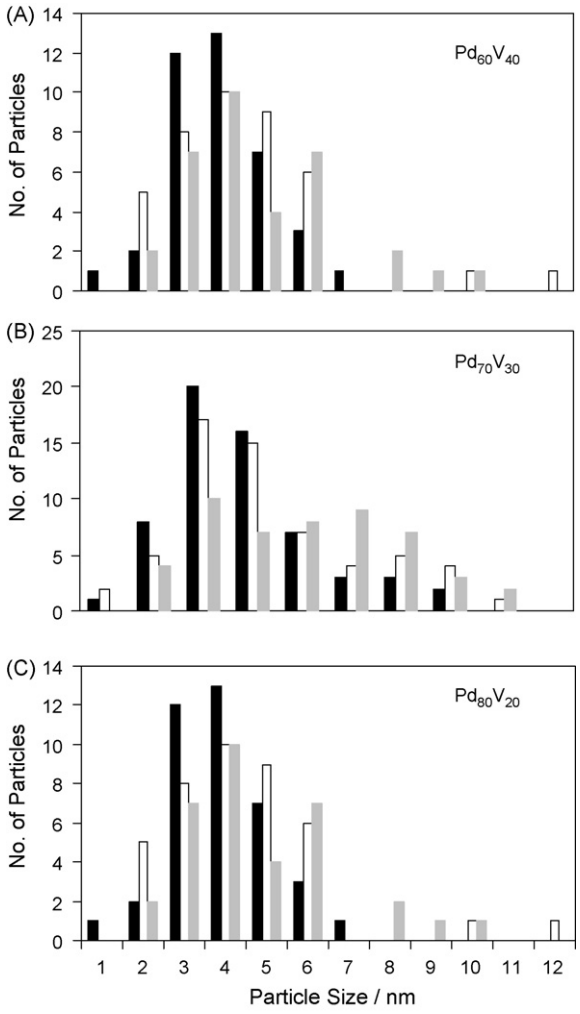

Fig. 2. Particle size distributions of each PdV/C electrocatalyst. The catalyst compositions are (from top to bottom) $Pd_{60}V_{40}$, $Pd_{70}V_{30}$ and $Pd_{80}V_{20}$. The black bars are the as-prepared electrocatalysts, the white bars are those treated at 300 °C and the grey bars are those treated at 500 °C. The distributions were determined by measuring 50 individual particles using TEM.

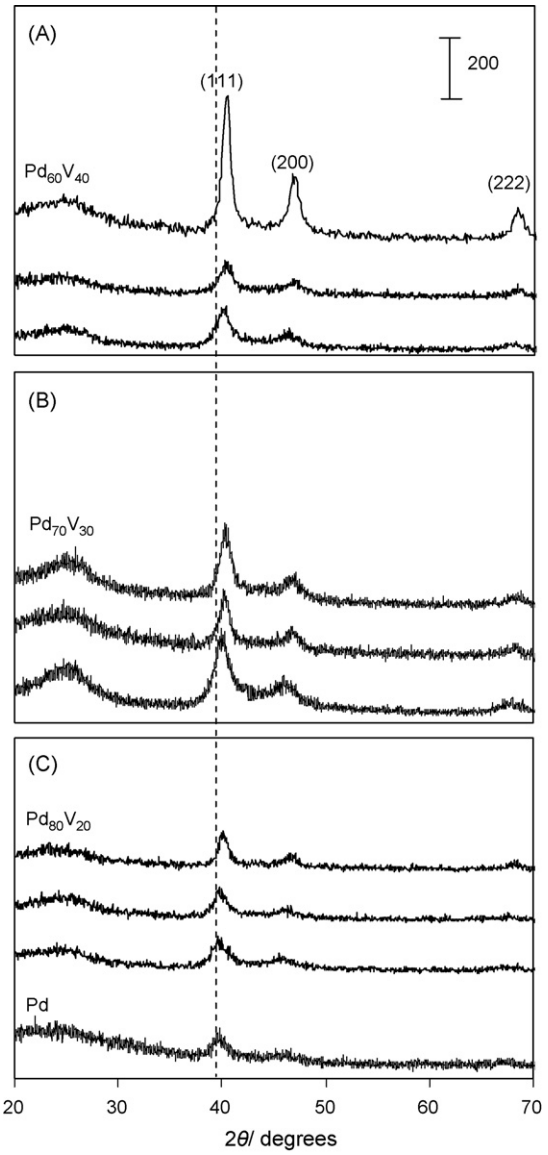

Fig. 3. XRD pattern of each PdV/C electrocatalyst. The catalyst compositions are (A) $Pd_{60}V_{40}$, (B) $Pd_{70}V_{30}$ and (C) $Pd_{80}V_{20}$. Within each frame, the samples are (from top to bottom) those treated at 500 °C, 300 °C and the as-prepared sample, respectively. The pattern obtained for pure Pd is shown in the bottom frame. The scale bar shows 200 arbitrary intensity units.

O_2-saturated 0.5 M H_2SO_4. At each electrocatalyst, mixed kinetic-diffusion control was observed at all potentials, as has also been observed during ORR at Pd alloyed with Ni [14]. The curves demonstrate significant changes in the electrocatalyst activities after treating at various temperatures. Decreases in the electrocatalytic activity are indicated by a shift in the curve to more negative potentials (higher ORR overpotentials). Conversely, increases in the electrocatalytic activity are indicated by shifts of the polarization curves to more positive potentials (lower ORR overpotentials). In our analysis, we used the electrocatalytic current, measured at +0.7 V, to quantify the electrocatalytic activity of each electrocatalyst. Table 2 contains the currents measured at each electrocatalyst at 0.7 V, as well as the surface area normalised current densities. The surface area in each case was calculated using Eq. (1):

$$S = \frac{6000}{d\rho} \quad (1)$$

where d is the particle size as calculated from XRD and ρ is the density of the electrocatalyst. The densities of $Pd_{60}V_{40}$, $Pd_{70}V_{30}$ and $Pd_{80}V_{20}$ were (calculated as a simple ratio of the densities of the metals in each composition) 9.66 g cm^{-3}, 10.25 g cm^{-3} and 10.84 g cm^{-3}, respectively. In general, heating treating at 300 °C and 500 °C caused a decrease in the surface area due to the increase in particle size upon heating. In the case of the $Pd_{60}V_{40}$ samples, the AP sample exhibited the highest activity for the ORR. The currents measured at +0.7 V were 0.312 mA and 0.0281 mA for the $Pd_{60}V_{40}$(AP) and $Pd_{60}V_{40}$(300) samples, respectively, demonstrating a significant decrease in electrocatalytic activity after heating at 300 °C. While heating the sample at 500 °C also caused a decrease in the electrocatalytic activity compared to the AP sample, the decrease was not as large as that observed when treated at 300 °C. In the $Pd_{70}V_{30}$ electrocatalyst, heating at 300 °C caused a substantial increase in the current at 0.7 V from 0.0862 mA (in the AP sample) to 0.420 mA, a 360% increase. However, when $Pd_{70}V_{30}$ was treated at 500 °C, the current was 0.0872 mA at 0.7 V but at higher overpotentials $Pd_{70}V_{30}$(500) produced lower currents. Finally, in the $Pd_{80}V_{20}$ electrocatalyst, the current at 0.7 V increased from 0.0897 mA to 0.156 mA upon heating at 300 °C, a current increase of 73%, but the current at $Pd_{80}V_{20}$(500) was only 0.0264 mA. The surface area nor-

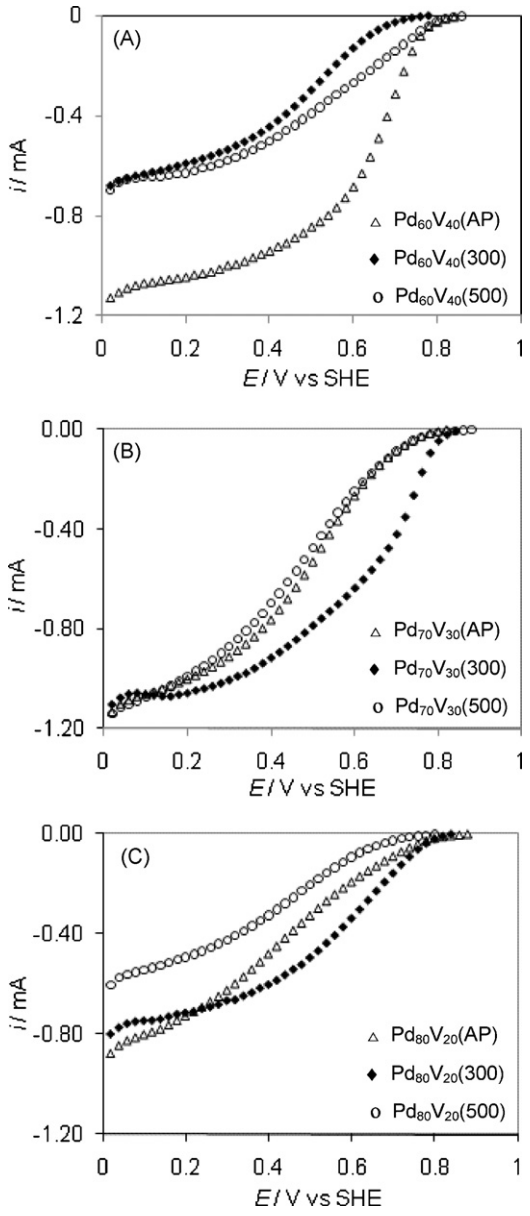

Fig. 4. Comparison of the polarisation curves obtained using each electrocatalyst in O_2-saturated 0.5 M H_2SO_4 at 25 °C. The potential was scanned from 0.9 V to 0.0 V at 5 mV s^{-1} and the electrode rotation rate was 1600 rpm. (A) $Pd_{60}V_{40}$, (B) $Pd_{70}V_{30}$ and (C) $Pd_{80}V_{20}$.

malised current densities in Table 2 show that the decrease and increase in the electrocatalytic activities of the various electrocatalysts is not simply related to changes in the surface area. Fig. 5 shows a comparison of polarisation curves obtained at the most active

Table 2
The change in surface area of the electrocatalysts and the current density measured at 0.7 V upon heat treatment at 300 °C and 500 °C. AP is the as-prepared sample at each composition.

Sample	i (μA) (at +0.7 V)	S (m^2 g^{-1})	j (μA cm^{-2})
$Pd_{60}V_{40}$(AP)	312	107.13	72.8
$Pd_{60}V_{40}$(300)	28.1	97.09	7.24
$Pd_{60}V_{40}$(500)	142	66.10	53.7
$Pd_{70}V_{30}$(AP)	86.2	95.99	22.5
$Pd_{70}V_{30}$(300)	420	81.32	129
$Pd_{70}V_{30}$(500)	87.2	88.72	24.6
$Pd_{80}V_{20}$(AP)	89.7	102.52	21.9
$Pd_{80}V_{20}$(300)	156	79.09	49.3
$Pd_{80}V_{20}$(500)	26.4	61.51	10.7

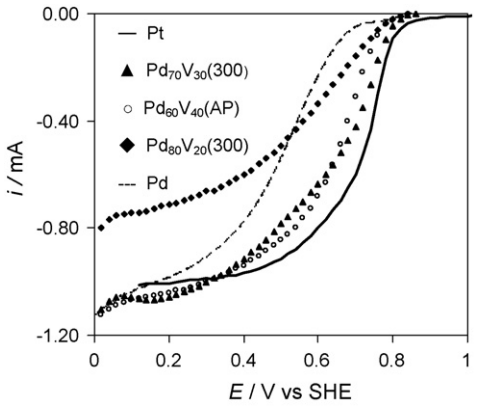

Fig. 5. Comparison of polarisation curves obtained using $Pd_{60}V_{40}$(AP), $Pd_{70}V_{30}$(300) and $Pd_{80}V_{20}$(300) electrocatalysts in O_2-saturated 0.5 M H_2SO_4 at 25 °C and 1600 rpm. Also shown are the curves obtained using Pd/C and commercial Pt/C (from Johnson Matthey). In each case the potential was swept in a negative potential direction at 5 mV s^{-1}.

electrocatalyst for each composition (60:40, 70:30 and 80:20). Also shown for comparison is the response obtained at a commercial Pt electrocatalyst (20 wt.% Pt/C from Johnson–Matthey) and a pure Pd/C electrocatalyst (20 wt.% prepared by $NaBH_4$ reduction of $PdCl_2$ in the presence of Vulcan XC72R). The commercial Pt electrocatalyst exhibited the highest onset ORR potential as well as the highest current between +0.8 V and +0.4 V whereas the pure Pd electrocatalyst exhibited the lowest current in the same region. $Pd_{70}V_{30}$(300) and $Pd_{60}V_{40}$(AP) showed significantly higher currents than pure Pd at all potentials and had a comparable onset potential to pure Pt. However, at higher overpotentials, pure Pt was clearly more active than all other electrocatalysts, which is perhaps not surprising considering the well-known high activity of Pt for the ORR.

The enhancement of electrocatalytic activity of Pd-based alloys has been attributed to a range of factors including changes in the interatomic spacing [20] and the surface electronic structure [21,22]. Heat treatment of alloy electrocatalysts has been shown to enhance the degree of alloying (as indicated by the decrease in lattice parameter) and the ORR catalytic activity [14]. In the cases of $Pd_{80}V_{20}$ and $Pd_{70}V_{30}$, the highest ORR activity was obtained after the samples were heat treated at 300 °C. In contrast, in the case of the $Pd_{60}V_{40}$ sample, heat treatment at 300 °C decreased the electrocatalytic activity of the as-prepared sample. Although the role of particle size in the activity of Pd-based ORR electrocatalysts is not fully understood, it is unlikely that the decrease in the activities of $Pd_{60}V_{40}$, and the increase in the activity of $Pd_{70}V_{30}$ and $Pd_{80}V_{20}$, upon heating at 300 °C are due to the increase in the average particle size, which was very small in each case. In addition, no clear correlation between the lattice parameters and the electrocatalytic activity is evident. It appears that, in some compositions, alloying at higher temperatures induces the formation of an optimum surface composition (specifically in the cases of $Pd_{70}V_{30}$ and $Pd_{80}V_{20}$), as was recently suggested for PdNi alloys [14]. However, these issues are clearly complicated and further experimental and theoretical work is required to fully understand the effect of each factor on electrocatalytic activity.

3.3. Electrochemical stability of PdV/C electrocatalysts

To study the electrochemical stability of the electrocatalysts, the electrocatalysts were subjected to an accelerated stability test by electrochemical cycling in deoxygenated 0.5 M H_2SO_4 between +0.4 V and +0.9 V 500 times at 0.5 V s^{-1}. Fig. 6 shows the cyclic voltammograms (CVs) of the $Pd_{60}V_{40}$(AP), $Pd_{70}V_{30}$(300) and $Pd_{80}V_{20}$(300) (the most active electrocatalysts at each nomi-

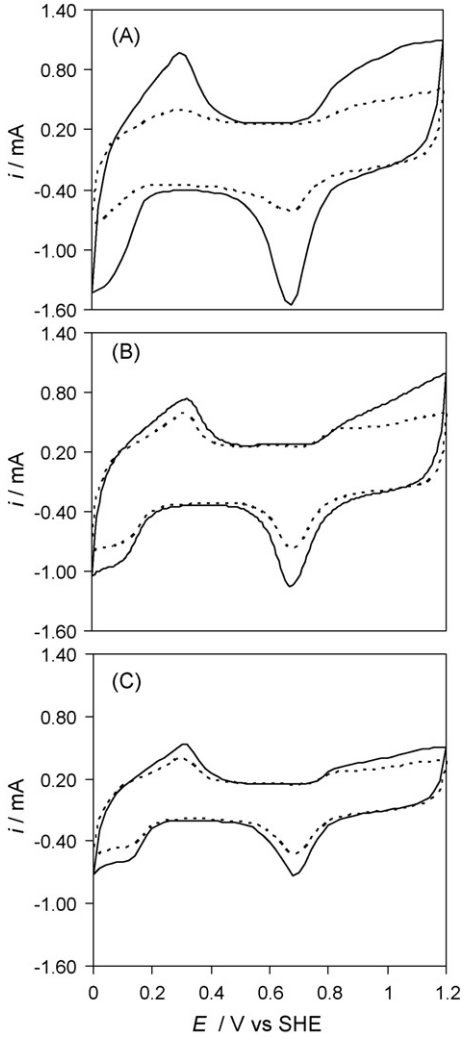

Fig. 6. Cyclic voltammograms obtained at (A) $Pd_{60}V_{40}$(AP), (B) $Pd_{70}V_0$(300) and (C) $Pd_{80}V_{20}$(300) in deoxygenated 0.5 M H_2SO_4 at 25 °C before (solid line) and after (dashed line) 500 cycles between 0.9 V and 0.4 V at 0.5 V s^{-1}. The CVs were recorded by sweeping the potential between 0.0 V and 1.2 V at 0.5 V s^{-1} in 0.5 M H_2SO_4.

nal composition) before and after the accelerated stability test. The shapes of the CVs before and after electrochemical cycling were typical of that expected for a Pd-based material in acidic media [7]. Estimation of the electrochemical surface area from the charge passed in the hydrogen absorption area is complicated by absorption of hydrogen into the Pd [14] and the presence of V in the electrocatalyst. Therefore, the change in the charge passed during the reduction of the metal oxide peak as the catalysts were electrochemically cycled was used as an indication of the change in the electrochemical surface area (ECSA) over time [7]. Fig. 6A shows that $Pd_{60}V_{40}$(AP) exhibited a significant loss of ECSA upon potential cycling and only retained about 25% of its initial ECSA. However, $Pd_{70}V_{30}$(300) retained 68% of its initial ECSA (Fig. 6B). $Pd_{80}V_{20}$(300) exhibited the highest stability retaining 80% of its initial ESCA (Fig. 6C), demonstrating that higher Pd contents improve the electrochemical stability. However, the stability of the $Pd_{80}V_{20}$ electrocatalyst is accompanied by a relatively poor electrocatalytic activity (described previously). Therefore, while $Pd_{60}V_{40}$ (AP) and $Pd_{70}V_{30}$ (300) showed comparable electrocatalytic activities prior to the stability test, $Pd_{70}V_{30}$(300) is clearly more resistant to loss of ECSA under potential cycling and is a more promising ORR electrocatalyst.

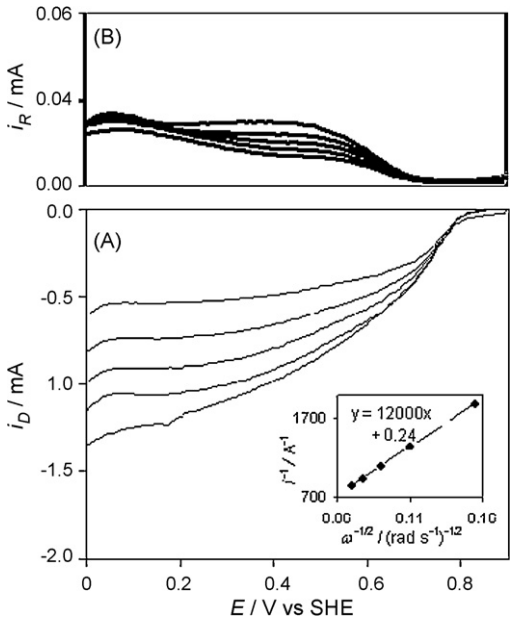

Fig. 7. (A) Polarisation curves obtained at $Pd_{70}V_{30}$(300) in O_2-saturated 0.5 M H_2SO_4 at (from top to bottom) 400 rpm, 800 rpm, 1200 rpm, 1600 rpm and 2000 rpm. The potential was swept from 0.9 V to 0.0 V at 5 mV s^{-1}. The corresponding Koutecky–Levich plot of i_L^{-1} vs $\omega^{-1/2}$ is shown in the inset. (B) Ring current measured at 1.2 V as the disk potential was swept from 0.9 V to 0.0 V.

3.4. Mechanism of oxygen reduction at $Pd_{70}V_{30}$(300)

The ORR can proceed by a direct 4-electron route to H_2O or by a 2-electron route producing H_2O_2. In the development of fuel cell electrocatalysts, the direct 4-electron ORR route is more preferable than the 2-electron route as the standard potential for the 4-electron route is significantly higher (1.23 V) than that of the 2-electron route (0.695 V). In addition, H_2O_2 can be homolysed on noble metals generating hydroxyl radicals and, Nafion, a commonly used polymer electrolyte in fuel cells, is susceptible to attack by hydroxyl radicals. In this study, we used RDE voltammetry to study the mechanism of ORR at the $Pd_{70}V_{30}$ electrocatalyst surface. The Koutecky–Levich equation relates the current at the RDE, i, to the rotation rate:

$$\frac{1}{i} = \frac{1}{nFkC} + \frac{1}{0.62nFAD^{2/3}C\nu^{-1/6}\omega^{1/2}} \quad (2)$$

where n is the number of electrons transferred during the reaction, F is the Faraday constant, k is the electron transfer rate constant, A is the electrode area, ν is the kinematic viscosity of the electrolyte, ω is the rotation rate and C and D are the concentration and diffusion coefficient of dissolved O_2 (1.22 mM and 1.93×10^{-5} cm^2 s^{-1}, respectively [23]). Fig. 7 shows RDE polarization curves recorded at the $Pd_{70}V_{30}$(300) electrocatalyst at different rotation rates. O_2 reduction began at approximately +0.82 V and the current increased with increasing rotation rate. n was calculated from slope of the Koutecky–Levich plot (Fig. 7, inset) and was 4.1 at $Pd_{70}V_{30}$(300). RRDE measurements were also used to determine n and Fig. 7 also shows the ring current (measured at 1.2 V to detect H_2O_2) as the disk potential was swept from 0.9 V to 0.0 V. n can be calculated using the equation:

$$n_e = \frac{4i_D}{i_D + (i_R/N)} \quad (3)$$

where i_D is the limiting current at measured at the disk, i_R is the current recorded at the ring and N is the collection efficiency of the ring (20%). From Eq. (3), n = 3.8 (at 1600 rpm), for $Pd_{70}V_{30}$(300),

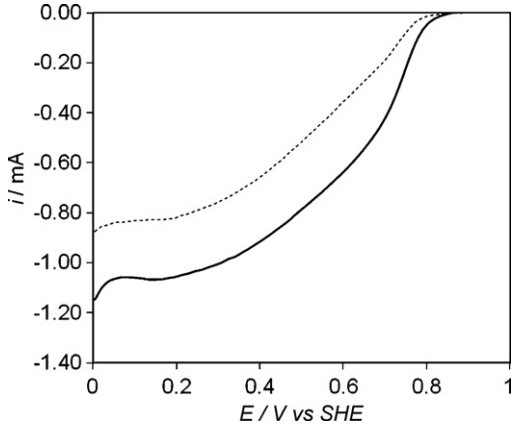

Fig. 8. Polarisation curves recorded at $Pd_{70}V_{30}$(300) before (solid line) and after (dashed line) cycling the potential between 0.9 V and 0.4 V 500 times in 0.5 M H_2SO_4. The conditions are as described in Fig. 5.

which is very close to the value obtained from the Koutecky–Levich analysis. Therefore, these results show that the ORR proceeded predominantly via the direct 4-electron pathway on $Pd_{70}V_{30}$(300) producing H_2O.

3.5. Effect of potential cycling on electrocatalytic performance and morphology of $Pd_{70}V_{30}$(300)

Fig. 8 shows ORR polarisation curves obtained using the most active electrocatalyst, $Pd_{70}V_{30}$, before and after potential cycling between 0.9 V and 0.4 V 500 times. There is a clear decrease in electrocatalytic activity after the stability test as indicated by a shift in the entire curve to more negative potentials. The current at 0.7 V prior to the stability test was 0.420 mA, which decreased to 0.19 mA, a 55% decrease. The loss of electrocatalyst activity during the ORR is well documented and is generally attributed to growth of the catalyst particles, loss of ECSA, corrosion of the carbon support and leaching of metal into the acid [9,23–25]. The morphology of the electrocatalyst after the stability test was examined by removing the catalyst layer from the GC surface, redispersing it in acetone (by shaking) and recording TEM images. Fig. 9 shows typical TEM images of $Pd_{70}V_{30}$ after potential cycling. Large areas of bare carbon were visible, in which metallic particles were not found (Fig. 9A). It is possible that this loss of metal is a result of nanoparticles being dislodged from the carbon after removal from the electrode surface and dispersion in acetone. However, in those locations where metallic particles were observed, the particles exhibited substantial growth. For example, Fig. 9B shows particles with diameters up to approximately 30 nm, which are significantly larger than the particles shown in Fig. 1. It is not clear from these images whether these larger structures are agglomerations of individual nanoparticles or whether these are individual particles that had grown. Nonetheless, it is clear that significant morphological changes occurred during the accelerated stability test, which probably contributed to the decreased ECSA (Fig. 6) and the loss of electrocatalytic activity (Fig. 8). However, the contribution of metal leaching from the alloy cannot be discounted and will be the focus of future work in this area. The relative instability of palladium alloys in acidic environments is not unusual [7] and has implications for the use of these materials in operational fuel cells. In the case of these palladium–vanadium alloys, it is clear that heat treatment is essential to enhance the stability of these materials but further work is required to optimise the lifetime and performance of these and other Pd-based ORR electrocatalysts.

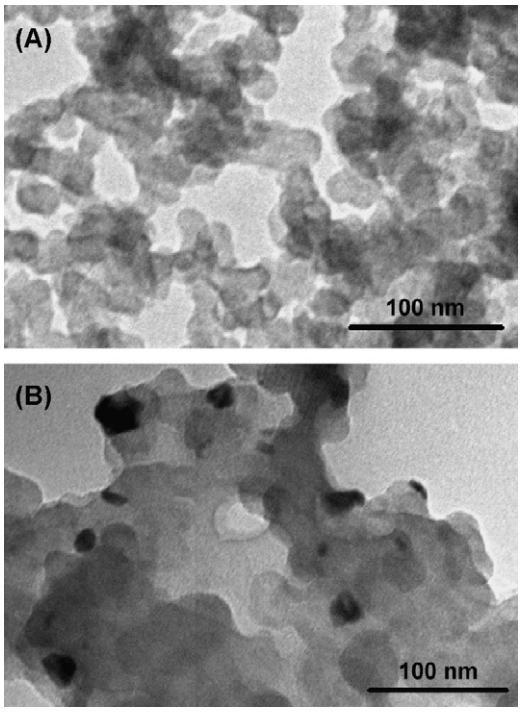

Fig. 9. TEM images of $Pd_{70}V_{30}$/C after cycling the potential 500 times between 0.9 V and 0.4 V in 0.5 M H_2SO_4.

4. Conclusions

A range of palladium–vanadium alloys for oxygen reduction have been synthesized by chemical reduction of metal salts in aqueous solution. Upon synthesizing the electrocatalysts, PdV at an atomic ratio of 60:40 exhibited the highest activity for oxygen reduction. However, after heat treating the electrocatalysts, major differences in the electrocatalytic performance and electrochemical stability of each electrocatalyst were revealed. From our results, it is clear that PdV at a ratio of 70:30, and heat treated at 300 °C, is the most promising PdV oxygen reduction electrocatalyst, both in terms of initial electrocatalytic activity and stability. However, significant morphological changes in the electrocatalyst can also be observed upon potential cycling, which include loss of metal from the carbon support as well as growth of the electrocatalyst particles. Therefore, considerably more work is required to improve the stability of these Pd-based materials if they are to replace state-of-the-art Pt-based materials as electrocatalysts for oxygen reduction in fuel cells.

Acknowledgements

We thank the UK Engineering and Physical Sciences Research Council for funding this work through the DICE (Driving Innovation in Chemistry and Chemical Engineering) Project under the Science and Innovation Award (Grant Number EP/D501229/1).

References

[1] W. Li, W. Zhou, H. Li, Z. Zhou, B. Zhou, G. Sun, Q. Xin, Electrochim. Acta 49 (2004) 1045.
[2] B. Lim, M. Jiang, P.H.C. Camargo, E.C. Cho, J. Tao, X. Lu, Y. Zhu, Y. Xia, Science 324 (2009) 1302.
[3] U.A. Paulus, A. Wokaun, G.G. Scherer, T.J. Schmidt, V. Stamenkovic, V. Radmilovic, N.M. Markovic, P.N. Ross, J. Phys. Chem. B 106 (2002) 4181.
[4] S. Pylypenko, S. Mukherjee, T.S. Olson, P. Atanassov, Electrochim. Acta 53 (2008) 7875.
[5] F. Jaouen, S. Marcotte, J.-P. Dodelet, G. Lindbergh, J. Phys. Chem. B 107 (2003) 1376.

[6] A. Sarkar, A.V. Murugan, A. Manthiram, J. Phys. Chem. C 112 (2008) 12037.
[7] H. Liu, W. Li, A. Manthiram, App. Catal. B-Environ. 90 (2009) 184.
[8] J.L. Fernandez, V. Raghuveer, A. Manthiram, A.J. Bard, J. Am. Chem. Soc. 127 (2005) 13100.
[9] R. Borup, J. Meyers, B. Pivovar, Y.S. Kim, R. Mukundan, N. Garland, D. Myers, M. Wilson, F. Garzon, D. Wood, P. Zelenay, K. More, K. Stroh, T. Zawodzinski, J. Boncella, J.E. McGrath, M. Inaba, K. Miyatake, M. Hori, K. Ota, Z. Ogumi, S. Miyata, A. Nishikata, Z. Siroma, Y. Uchimoto, K. Yasuda, K.I. Kimijima, N. Iwashita, Chem. Rev. 107 (2007) 3904.
[10] K. Yasuda, A. Taniguchi, T. Akita, T. Ioroi, Z. Siroma, J. Electrochem. Soc. 153 (2006) A1599.
[11] Y.Y. Shao, R. Kou, J. Wang, V.V. Viswanathan, J.H. Kwak, J. Liu, Y. Wang, Y.H. Lin, J. Power Sources 185 (2008) 280.
[12] P.J. Ferreira, G.J.O'.l.Y. Shao-Horn, D. Morgan, R. Makharia, S. Kocha, H.A. Gasteiger, J. Electrochem. Soc. 152 (2005) A2256.
[13] E. Antolini, Energy Environ. Sci. 2 (2009) 915.
[14] J. Zhao, A. Sarkar, A. Manthiram, Electrochim. Acta 55 (2010) 1756.
[15] E. Antolini, R.R. Passos, E.A. Ticianelli, Electrochim. Acta 48 (2002) 263.
[16] J. Luo, N. Kariuki, L. Han, L.Y. Wang, C.H. Zhong, T. He, Electrochim. Acta 51 (2006) 4821.
[17] D.A. Walsh, J.L. Fernandez, A.J. Bard, J. Electrochem. Soc. 153 (2006) E99.
[18] C.W.B. Bezerra, L. Zhang, H. Liu, K. Lee, A.L.B. Marques, E.P. Marques, H. Wang, J. Zhang, J. Power Sources 173 (2007) 891.
[19] A. Weibel, R. Bouchet, F. Boulc, P. Knauth, Chem. Mater. 17 (2005) 2378.
[20] M.-H. Shao, K. Sasaki, R.R. Adzic, J. Am. Chem. Soc. 128 (2006) 3526.
[21] M. Shao, P. Liu, J. Zhang, R. Adzic, J. Phys. Chem. B 111 (2007) 6772.
[22] S. Vojislav, M. Bongjin Simon, J.J.M. Karl, N.R. Philip, M.M. Nenad, R. Jan, G. Jeff, K.N. Jens, Angew Chem. Int. Ed. 45 (2006) 2897.
[23] S.-Y. Ang, D.A. Walsh, J. Power Sources 195 (2010) 2557.
[24] S.C. Zignani, E. Antolini, E.R. Gonzalez, J. Power Sources 182 (2008) 83.
[25] R.L. Borup, J.R. Davey, F.H. Garzon, D.L. Wood, M.A. Inbody, J. Power Sources 163 (2006) 76.